Rapid Communications

# Excitonic enhancement of optical nonlinearities in perovskite $CH_3NH_3PbCl_3$ single crystals

Keiichi Ohara,[1] Takumi Yamada,[1] Hirokazu Tahara,[1] Tomoko Aharen,[1] Hideki Hirori,[1] Hidekatsu Suzuura,[2] and Yoshihiko Kanemitsu[1,*]

[1]*Institute for Chemical Research, Kyoto University, Uji, Kyoto 611-0011, Japan*

[2]*Graduate School of Engineering, Hokkaido University, Sapporo, 060–8628, Japan*

(Received 22 May 2019; published 6 November 2019)

Metal halide perovskites have emerged as versatile photonic device materials because of their outstanding band structure and excellent optical properties. Here, we determined the excitation wavelength dependences of the two-photon absorption coefficient and the Kerr-effect-induced nonlinear refractive index of $CH_3NH_3PbCl_3$ perovskite single crystals by means of the *Z*-scan method. From theoretical analysis, we found that the electron-hole interaction, so-called exciton effect, significantly enhances the nonlinear optical responses even for the interband transitions. This interaction explains the universal relation between the exciton reduced mass and the bandgap for lead halide perovskites.

DOI: 10.1103/PhysRevMaterials.3.111601

Lead halide perovskites are actively studied as materials for optical devices such as solar cells and light emitting diodes [1–9]. The material and optoelectronic properties of perovskites, which have a crystal structure described by $APbX_3$, can be easily modified by changing the cation element at the *A* site or the halogen at the *X* site [10,11]. Intensive investigations have revealed that lead halide perovskites belong to the class of direct-gap semiconductors. They feature a low density of defects and traps in the band gap, extremely high luminescence efficiencies in the visible and near-infrared wavelength regions, a sharp absorption edge, and a large absorption coefficient [12–18]. Current areas of investigation include the impact of the Rashba effect on the near-band-edge structure [19,20] and the role of the bright triplet excitons originating from the lowest spin split-off conduction band on optical responses [21]. Lead halide perovskites possess new and unconventional optical characteristics, and as a result, they are also attracting much attention in the area of fundamental physics.

Very recently, nonlinear optical phenomena, such as lasing [22,23] and optical modulation [24], as well as for high-order harmonic generation [25] have been reported for perovskites. Since material transparency constitutes an important factor for nonlinear optics, the wide-gap semiconductors [$APbX_3$($X$ = Br, Cl), e.g., $CH_3NH_3PbCl_3$] have been widely studied [26–29]. A more detailed understanding of their nonlinear optical coefficients is required to elucidate the origin of complex optical phenomena observed in these wide-gap perovskites. In addition, we note that these materials possess a simple but unique band structure that enables straightforward analysis by theoretical calculations. Consequently, the accurate determination of the optical coefficients and their model band structure may be considered as a useful example case for examining the fundamental photophysics of semiconductors. There is, however, considerable variation in the reported values of nonlinear optical coefficients [30]. To determine the intrinsic nonlinear optical coefficients, we employ a single crystal sample with a flat surface and a low defect density [10,31,32].

In this Rapid Communication, we study the third-order nonlinear optical coefficients of a wide-gap semiconductor $CH_3NH_3PbCl_3$ single crystal by using the *Z*-scan method. The nonlinear optical properties at the band edge were examined by measuring the excitation-wavelength dependences of the nonlinear optical coefficients. The nonlinear optical properties were analyzed using Kane's $k \cdot p$ method and a direct-gap two-band model that accounts for the exciton effect. This model enabled determination of the Kane energy and the exciton reduced mass. We found that the value of the nonlinear optical coefficient of $CH_3NH_3PbCl_3$ is enhanced by the exciton effect.

The $CH_3NH_3PbCl_3$ single crystal samples used in this work were prepared by antisolvent vapor-assisted crystallization [31]. Figure 1(a) is a photograph of a representative sample to illustrate the size and transparency of the crystals obtained by this growth method. A back-reflection Laue photograph of such $CH_3NH_3PbCl_3$ single crystals is shown in Fig. 1(b). The details of the Laue measurement are given in the Supplemental Material [33]. Figure 1(b) clarifies that the crystal is in the cubic phase and the sample's surface orientation is (100). Also, the recorded Laue spots clearly indicate that the sample is a high-quality single crystal. For the optical measurements, we used cleaved single crystal samples (Fig. S1) to reduce the light scattering. The previously reported values of the nonlinear optical coefficients exhibit a large variation and accurate values have not yet been determined [30]. This is because many of the previous studies on lead halide perovskites employed polycrystalline thin films and nanocrystal samples, which are strongly affected by extrinsic factors such as light scattered by the grain structure of the surface and charging by surface traps.

*Corresponding author: kanemitu@scl.kyoto-u.ac.jp

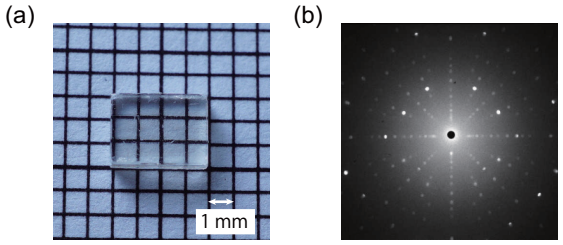


FIG. 1. (a) Representative $CH_3NH_3PbCl_3$ single crystal sample. (b) Back-reflection Laue photograph of a $CH_3NH_3PbCl_3$ single crystal, showing (100) orientation.

The *Z*-scan method [39,40] was used to determine both the nonlinear refractive index $\gamma$ induced by the optical Kerr effect and the two-photon absorption coefficient $\beta$. The experimental setup is shown in Fig. 2(a). Here, $\gamma$ and $\beta$ are related to the real and imaginary parts of the third-order nonlinear susceptibility $\chi^{(3)}$ [39]. In materials with inversion symmetry (like the present cubic perovskites), the second-order nonlinear susceptibility $\chi^{(2)}$ is zero, and thus the polarizability derived from $\chi^{(3)}$ is most significant for the nonlinear optical responses. The *Z*-scan method is advantageous for our purpose, because the absolute values (including sign) of $\gamma$ and $\beta$ can be measured separately and with high sensitivity by simply opening and closing the aperture in front of the detector. The former measurement geometry is the so-called open-aperture (OA) measurement and allows us to obtain $\beta$. The latter is the closed-aperture (CA) measurement, which provides $\gamma$ by observing the self-focusing or self-defocusing

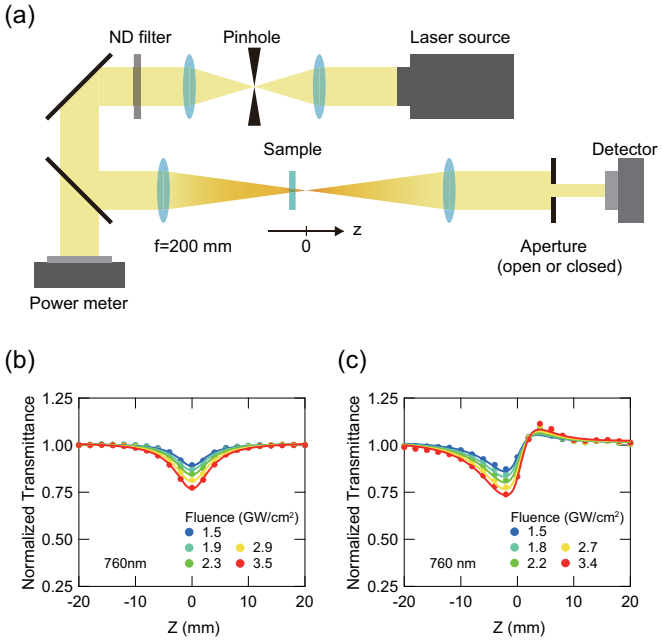


FIG. 2. (a) *Z*-scan setup. The details of the experimental setup are provided in the Supplemental Material [33]. Normalized transmittance for (b) the OA configuration and (c) the CA configuration. The experimental results and fitting curves are shown with dots and solid lines, respectively.

induced by the optical Kerr effect (see Supplemental Material [33]). By using a cleaved single crystal with a flat surface, we were able to significantly reduce the distortion of the Gaussian beam, and thus achieve accurate OA and CA measurements. Figure S1(b) in the Supplemental Material evidences the negligible beam distortion in our approach [33].

The excitation-fluence dependences of transmitted light intensities in the OA and CA configurations are shown in Figs. 2(b) and 2(c), respectively. Here, the excitation wavelength was 760 nm and the fluence was changed in the range from 1.5 to 3.5 $GW/cm^2$. We note that the excitation fluence of the incident laser is corrected by the surface reflection, $R = 0.1$. The horizontal axes in Figs. 2(b) and 2(c) represent the position of the sample, where the focal point is located at $z = 0$ and the sign is positive on the detector side [see Fig. 2(a)]. The vertical axis is the transmitted light intensity normalized by the intensity obtained at the end point of each $z$ scan ($z = 20$ mm) where the excitation fluence is significantly weak and the nonlinear optical effects are negligible. In both the OA and CA measurements, the signals due to the nonlinear responses near $z = 0$ become stronger with excitation fluence.

We also performed excitation-fluence dependence measurements for other wavelengths from 660 to 840 nm. The results are provided in the Supplemental Material (see Fig. S2). The data is evidence that a signal due to nonlinear absorption is observed only when the excitation wavelength is shorter than 800 nm, and as the excitation wavelength becomes shorter, the nonlinear absorption becomes stronger. These results reflect the fact that the band-gap energy of $CH_3NH_3PbCl_3$ corresponds to a wavelength near 400 nm [29], that is, the two-photon absorption edge appears near 800 nm. Figures 2(c) and S2(b) show that the amount of transmission decreases for sample positions $z < 0$ and increases for $z > 0$. This evidences that the self-focusing occurs and the nonlinear refractive index $\gamma$ is positive.

To determine the values of the third-order nonlinear optical coefficients $\beta$ and $\gamma$, we need to obtain the excitation-fluence dependences of the parameters $q_0$ and $\Delta\Phi_0$ from OA and CA measurements, respectively. Here, $q_0$ represents the ratio of the amount of nonlinear absorption to incident light intensity, and $\Delta\Phi_0$ represents the phase shift due to nonlinear refraction. By using appropriate fitting functions [39,40] (see Supplemental Material [33]), we successfully reproduced the OA and CA data as shown with the solid curves in Figs. 2 and S2. The obtained values of $q_0$ and $\Delta\Phi_0$ are plotted in Figs. 3(a) and 3(b), respectively. Since $q_0$ and $\Delta\Phi_0$ are linearly proportional to the excitation fluence $I_0$, $\beta$ and $\gamma$ can be obtained from the following relations: $q_0 = \beta I_0 L$ and $\Delta\Phi_0 = k\gamma I_0 L$ [39,40]. Here, $L$ is the sample thickness $L = 1.41$ mm and $k$ is the wave number, defined by $\frac{2\pi}{\lambda}$. The experimentally observed linear relations clearly show that the third-order nonlinearity is dominant.

Furthermore, in order to verify that heating effect does not play an essential role in the nonlinear optical responses in our experimental condition, we performed the *Z*-scan measurements with different laser repetition rates with the same pulse energy. The laser repetition-rate dependences of the OA and CA measurements are shown in Figs. 3(c) and 3(d), respectively. In general, the temperature rise induced by laser irradiation increases as the repetition rate is increased. In spite

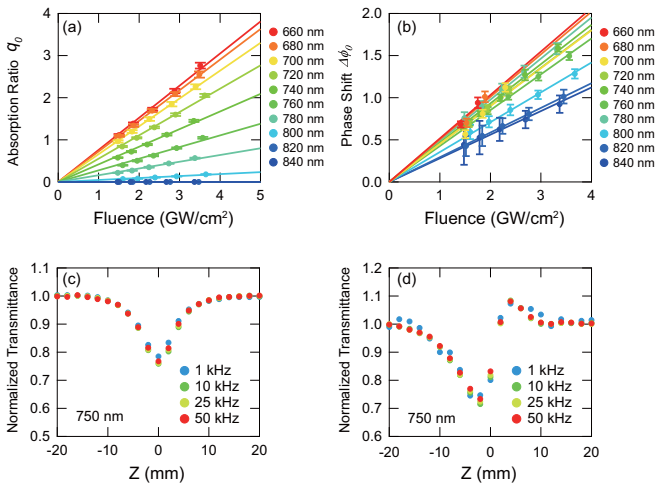


FIG. 3. Excitation-fluence dependences of (a) absorption ratio $q_0$ obtained from the OA measurements and (b) phase shift $\Delta\Phi_0$ obtained from the CA measurements at various wavelengths. Laser repetition-rate dependence of the signals in (c) the OA measurements and (d) the CA measurements. The repetition rate is varied in the range from 1 to 50 kHz.

of this, no changes are observed in the OA and CA measurements shown in Figs. 3(c) and 3(d). These results indicate that heating effects are sufficiently suppressed at the 10 kHz used in this study. Therefore, we conclude that the two-photon absorption coefficients $\beta$ and the Kerr-effect-induced nonlinear refractive index $\gamma$ can be precisely determined by the present $Z$-scan measurements.

In Fig. 4, the obtained third-order nonlinear optical coefficients $\beta$ and $\gamma$ are plotted against the excitation photon energy. The two-photon absorption starts to occur around photon energies that correspond to half of the band-gap energy of $CH_3NH_3PbCl_3$, and the absorption becomes stronger for higher energies. The magnitudes of $\beta$ and $\gamma$ of this wide-gap perovskite are larger than those of conventional wide- and direct-gap semiconductors [41].

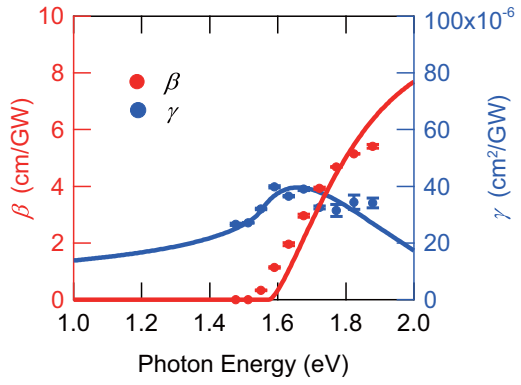


FIG. 4. Excitation-energy dependences of the two-photon absorption coefficient $\beta$ (red, scale on the left) and the Kerr-effect-induced nonlinear refractive index $\gamma$ (blue, scale on the right). The horizontal axis is the photon energy of the excitation laser. Red and blue solid lines indicate the fitting results obtained without considering the exciton effect.

The information on the electronic structure and optical responses of $CH_3NH_3PbCl_3$ can be obtained by analyzing the excitation-energy dependence of the experimental data shown in Fig. 4. Lead halide perovskites are known to have a direct-gap band structure composed of a $s$-like valence band and a $p$-like conduction band [42,43]. In addition, the conduction band is split due to the large spin–orbit interaction, and the spin split-off band with a total angular momentum $J = \frac{1}{2}$ constitutes the bottom of the conduction band. In case of linearly polarized excitation, the band edge can be well approximated by an ideal nondegenerate direct-gap two-band model. Furthermore, the values of the effective masses of electron and hole are nearly equal [21].

The excitation-wavelength dependences of the third-order nonlinear optical coefficients $\beta$ and $\gamma$ in the vicinity of the two-photon resonance for the nondegenerate two-band model has been previously derived [44,45]:

$$\beta = \frac{K\sqrt{E_p}}{n_0^2 E_g^3} F\left(\frac{\hbar\omega}{E_g}\right), \tag{1}$$

$$\gamma = \frac{K\sqrt{E_p}}{2n_0^2 E_g^4} G\left(\frac{\hbar\omega}{E_g}\right). \tag{2}$$

Here, $F$ and $G$ are dimensionless functions (see Supplemental Material [33]), $n_0$ is the linear refractive index, $E_g$ is the band-gap energy, and $K$ is a constant reflecting the character of valence and conduction bands. For the lead halide perovskites, interband transitions take place between the s-like valence band with $S = \frac{1}{2}$ and the conduction band with $J = \frac{1}{2}$ and the transition matrix moments are isotropic. We theoretically obtain $K = 1867$ by taking into account such isotropic matrix elements and the reduced mass within the $k \cdot p$ theory (see Supplemental Material [33]). In conventional semiconductors, the band edges are complex due to the degeneracy and spin–orbit interactions. Nevertheless, the band edge has been approximated by a two-band model [44,45], and this makes usage of empirical values for the factor $K = 3100$ in Eqs. (1) and (2) necessary. On the other hand, in the perovskites, the two-band model is valid to a high degree of accuracy. Therefore, we can expect that $K = 1867$ allows us to reproduce the experimental results. Note that the Coulomb interaction, or exciton effect, is not considered in this model. Finally, the Kane energy is defined by $E_p = \frac{2P^2}{m_0}$. Here, $P$ is the so-called Kane parameter which is originally defined by the matrix elements between the $s$-like state $|S\rangle$ and the $p$-like states $|X\rangle, |Y\rangle, |Z\rangle$, that is, $P = i\langle X|p_x|S\rangle = i\langle Y|p_y|S\rangle = i\langle Z|p_z|S\rangle$. The Kane energy is directly linked to the magnitude of the oscillator strength and is one of the most important physical parameters that characterize electronic structures as well as optical properties.

The excitation-energy dependences of $\beta$ and $\gamma$ are fitted with Eqs. (1) and (2), respectively, where $E_g = 3.15$ eV for $CH_3NH_3PbCl_3$ [29], $n_0 = 1.90$ [28], and the Kane energy $E_p$ is the common fitting parameter. The fitting results are shown in Fig. 4 with the red and blue solid lines. The experimentally observed wavelength dependence of $\beta$ cannot be reproduced with high accuracy. We confirmed that the used $E_g$ also provides a good fit for the ratio of $\gamma$ to $\beta$ which is equal to $2E_gG/F$, i.e., independent of $E_p$. Using the

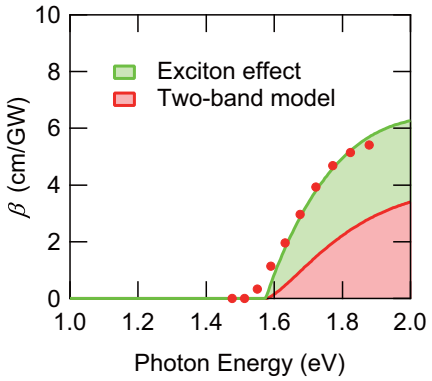


FIG. 5. The green solid line is the fitting result considering the exciton effect. The green area represents the contribution from the exciton effect, and the red area represents the contribution from the two-band model.

above model, we obtained $E_p = 120 \pm 9$ eV, which is much larger than the nearly material-independent value of 21 eV for most direct-gap semiconductors [41,44]. We should regard this parameter $E_p$ as an "effective" Kane energy because the Coulomb interaction between electron and hole, namely, exciton effect, is not taken into consideration in this model.

It has been reported that the bound electron-hole pair (exciton) plays a major role in the linear optical responses of $CH_3NH_3PbCl_3$ around the absorption edge, and the exciton effect is also important for the continuum spectra due to interband transitions [29]. The exciton effect plays an important role for the two-photon absorption transition above the band-gap energy through the Coulomb interaction. This is because the Coulomb interaction causes larger values of the matrix elements for transitions generating electron-hole pairs. We note that the $1s$ exciton peak cannot be observed in the two-photon absorption spectrum at room temperature, because of the selection rule for optical transitions. Since the binding energy of $2p$ excitons is smaller than the room-temperature thermal energy, $2p$ excitons are not observed in the two-photon absorption spectra [29]. In order to consider the exciton effect, it is necessary to incorporate the so-called Sommerfeld factor, that is $C(\omega) = x\frac{e^x}{\sinh x}$ [46], into Eq. (1) where $x = \pi\sqrt{\frac{E_b}{2\hbar\omega - E_g}}$ with $E_b$ being the exciton binding energy. In this improved model, the exciton effect gives an additional factor $C(\omega)$ for the two-photon absorption coefficients $\beta$. In materials with large exciton binding energy, this Sommerfeld factor also affects the two-photon transition at energies much higher than the band-gap energy. By performing the fit based on the model including the exciton effect with $E_b = 41$ meV and $E_g = 3.15$ eV [29], we obtain the green solid line in Fig. 5. Clearly, a better agreement with the experiment is realized and the actual Kane energy is given by $E_p = 23 \pm 1$ eV. This value is slightly larger than the value mentioned above, $E_p \approx 21$ eV [41,44]. The red area in Fig. 5 represents the contribution to $\beta$ from the two-band model for $E_p = 23$ eV without the exciton effect, and the green area represents the additional contribution due to the exciton effect. Figure 5 shows that the nonlinear optical coefficient is enhanced about twice by the exciton effect. The analysis clarifies that the exciton effect is quite important for the nonlinear optical responses of $CH_3NH_3PbCl_3$.

The large spin–orbit interactions in lead halide perovskites allow us to well explain the electron-hole dispersion by the 4 $\times$ 4 Kane model of the $s$-like valence band with $S = \frac{1}{2}$ spin degeneracy and the spin split-off conduction band with $J = \frac{1}{2}$ [21]. Then, by diagonalizing the Hamiltonian using Kane's $k \cdot p$ method, the relations between the Kane energy and the exciton reduced mass $\mu$ can be written as Eq. (S7) in the Supplemental Material [33]. Equation (S7) makes us understand the heavy exciton reduced mass in the lead halide perovskite. In this theory, by using the Kane energy $E_p = 23$ eV, the exciton reduced mass is estimated to $\mu = \frac{16}{E_g} = 0.20m_0$. In previous works [47–49], the exciton reduced masses of various narrow-gap metal halide perovskites including $CH_3NH_3PbI_3$ and $CH_3NH_3PbBr_3$ have been determined by magnetotransmission spectroscopy; the previously reported band-gap-energy dependence of $\mu$ is $\frac{m_0}{\mu} = \frac{17.3}{E_g}$. By employing $E_g = 3.15$ eV for $CH_3NH_3PbCl_3$, we obtain $\mu = 0.18m_0$, which is close to the above value. Because the theoretically extracted $\mu$ and the experimental $\mu$ are consistent, we found that this material can be accurately described by the two-band model and Kane's $k \cdot p$ method. In this way, by the analysis incorporating the exciton effect in optical nonlinearities, we are able to support the proposed simple universal relation between $E_g$ and $\mu$ for lead halide perovskites. Through our measurements, we succeeded in determining not only the nonlinear optical coefficients but also basic parameters that determine optical properties.

In conclusion, we studied the nonlinear optical response of a $CH_3NH_3PbCl_3$ single crystal using the $Z$-scan method. By considering the excitation-fluence dependence and the laser repetition-rate dependence, we succeeded in accurately determining the two-photon absorption coefficient $\beta$ and the Kerr-effect-induced nonlinear refractive index $\gamma$. From the excitation-energy dependences of these third-order nonlinear optical coefficients near the two-photon absorption edge, it was found that the values of $\beta$ and $\gamma$ are larger than those of conventional wide-gap semiconductors. Moreover, the analysis by a direct-gap two-band model incorporating the exciton effect clarified that the exciton effect is a very important factor for the nonlinear optical responses of $CH_3NH_3PbCl_3$. We determined the Kane energy $E_p = 23$ eV, which is an important physical parameter representing the oscillator strength, and the exciton reduced mass $= 0.20m_0$. Our findings show that $CH_3NH_3PbCl_3$ has a large optical transition probability and clarify its potential as an optical device material.

The authors thank Dr. T. Kikuchi of Rigaku Corporation for the x-ray Laue measurements. Sample preparation was supported by JST-CREST (Grant No. JPMJCR16N3). Part of the spectroscopic studies were supported by KAKENHI (Grants No. 18H03682, No. 19H05465, and No. 16K05391).

[1] A. Kojima, K. Teshima, Y. Shirai, and T. Miyasaka, J. Am. Chem. Soc. **131**, 6050 (2009).

[2] M. M. Lee, J. Teuscher, T. Miyasaka, T. N. Murakami, and H. J. Snaith, Science **338**, 643 (2012).

[3] W. S. Yang, B-W. Park, E. H. Jung, N. J. Jeon, Y. C. Kim, D. U. Lee, S. S. Shin, J. Seo, E. K. Kim, J. H. Noh, and S. I. Seok, Science **356**, 1376 (2017).

[4] D. Luo, W. Yang, Z. Wang, A. Sadhanala, Q. Hu, R. Su, R. Shivanna, G. F. Trindade, J. F. Watts, Z. Xu, T. Liu, K. Chen, F. Ye, P. Wu, L. Zhao, J. Wu, Y. Tu, Y. Zhang, X. Yang, W. Zhang, R. H. Friend, Q. Gong, H. J. Snaith, and R. Zhu, Science **360**, 1442 (2018).

[5] E. H. Jung, N. J. Jeon, E. Y. Park, C. S. Moon, T. J. Shin, T-Y. Yang, J. H. Noh, and J. Seo, Nature (London) **567**, 511 (2019).

[6] Z.-K. Tan, R. S. Moghaddam, M. L. Lai, P. Docampo, R. Higler, F. Deschler, M. Price, A. Sadhanala, L. M. Pazos, D. Credgington, F. Hanusch, T. Bein, H. J. Snaith, and R. H. Friend, Nat. Nanotechnol. **9**, 687 (2014).

[7] K. Lin, J. Xing, L. N. Quan, F. P. G. de Arquer, X. Gong, J. Lu, L. Xie, W. Zhao, D. Zhang, C. Yan, W. Li, X. Liu, Y. Lu, J. Kirman, E. H. Sargent, Q. Xiong, and Z. Wei, Nature (London) **562**, 245 (2018).

[8] Y. Cao, N. Wang, H. Tian, J. Guo, Y. Wei, H. Chen, Y. Miao, W. Zou, K. Pan, Y. He, H. Cao, Y. Ke, M. Xu, Y. Wang, M. Yang, K. Du, Z. Fu, D. Kong, D. Dai, Y. Jin, G. Li, H. Li, Q. Peng, J. Wang, and W. Huang, Nature (London) **562**, 249 (2018).

[9] T. Chiba, Y. Hayashi, H. Ebe, K. Hoshi, J. Sato, S. Sato, Y-J. Pu, S. Ohisa, and J. Kido, Nat Photonics **12**, 681 (2018).

[10] Y. Kanemitsu and T. Handa, Jpn. J. Appl. Phys. **57**, 090101 (2018).

[11] J-P. Correa-Baena, M. Saliba, T. Buonassisi, M. Grätzel, A. Abate, W. Tress, and A. Hagfeldt, Science **358**, 739 (2017).

[12] S. D. Stranks, G. E. Eperon, G. Grancini, C. Menelaou, M. J. P. Alcocer, T. Leijtens, L. M. Herz, A. Petrozza, and H. J. Snaith, Science **342**, 341 (2013).

[13] G. Xing, N. Mathews, S. Sun, S. S. Lim, Y. M. Lam, M. Grätzel, S. Mhaisalkar, and T. C. Sum, Science **342**, 344 (2013).

[14] Y. Yamada, T. Nakamura, M. Endo, A. Wakamiya, and Y. Kanemitsu, Appl. Phys. Express **7**, 032302 (2014).

[15] S. D. Wolf, J. Holovsky, S.-J. Moon, P. Löper, B. Niesen, M. Ledinsky, F.-J. Haug, J.-H. Yum, and C. Ballif, J. Phys. Chem. Lett. **5**, 1035 (2014).

[16] Y. Yamada, T. Nakamura, M. Endo, A. Wakamiya, and Y. Kanemitsu, J. Am. Chem. Soc. **136**, 11610 (2014).

[17] Q. Dong, Y. Fang, Y. Shao, P. Mulligan, J. Qiu, L. Cao, and J. Huang, Science **347**, 967 (2015).

[18] Y. Yamada, T. Yamada, L. Q. Phuong, N. Maruyama, H. Nishimura, A. Wakamiya, Y. Murata, and Y. Kanemitsu, J. Am. Chem. Soc. **137**, 10456 (2015).

[19] S. D. Stranks and P. Plochocka, Nat. Mater. **17**, 381 (2018).

[20] D. Niesner, M. Wilhelm, I. Levchuk, A. Osvet, S. Shrestha, M. Batentschuk, C. Brabec, and T. Fauster, Phys. Rev. Lett. **117**, 126401 (2016).

[21] M. A. Becker, R. Vaxenburg, G. Nedelcu, P. C. Sercel, A. Shabaev, M. J. Mehl, J. G. Michopoulos, S. G. Lambrakos, N. Bernstein, J. L. Lyons, T. Stöferle, R. F. Mahrt, M. V. Kovalenko, D. J. Norris, G. Rainò, and A. L. Efros, Nature (London) **553**, 189 (2018).

[22] G. Xing, N. Mathews, S. S. Lim, N. Yantara, X. Liu, D. Sabba, M. Grätzel, S. Mhaisalkar, and T. C. Sum, Nat. Mater. **13**, 476 (2014).

[23] H. Zhu, Y. Fu, F. Meng, X. Wu, Z. Gong, Q. Ding, M. V. Gustafsson, M. T. Trinh, S. Jin, and X-Y. Zhu, Nat. Mater. **14**, 636 (2015).

[24] H. Tahara, T. Aharen, A. Wakamiya, and Y. Kanemitsu, Adv. Opt. Mater. **6**, 1701366 (2018).

[25] H. Hirori, P. Xia, Y. Shinohara, T. Otobe, Y. Sanari, H. Tahara, N. Ishii, J. Itatani, K. L. Ishikawa, T. Aharen, M. Ozaki, A. Wakamiya, and Y. Kanemitsu, APL Mater. **7**, 041107 (2019).

[26] S. Yakunin, L. Protesescu, F. Krieg, M. I. Bondnarchuk, G. Nedelcu, M. Humer, G. D. Luca, M. Fiebig, W. Heiss, and M.V. Kovalenko, Nat. Commun. **6**, 8056 (2015).

[27] Y. Wang, X. Li, X. Zhao, L. Xiao, H. Zeng, and H. Sun, Nano Lett. **16**, 448 (2016).

[28] T. Handa, H. Tahara, T. Aharen, and Y. Kanemitsu, Sci. Adv. **5**, eaax0786 (2019).

[29] T. Yamada, T. Aharen, and Y. Kanemitsu, Phys. Rev. Lett. **120**, 057404 (2018).

[30] A. Ferrando, J. P. Martínez Pastor, and I. Suárez, J. Phys. Chem. Lett. **9**, 5612 (2018).

[31] D. Shi, V. Adinolfi, R. Comin, M. Yuan, E. Alarousu, A. Buin, Y. Chen, S. Hoogland, A. Rothenberger, K. Katsiev, Y. Losovyj, X. Zhang, P. A. Dowben, O. F. Mohammed, E. H. Sargent, and O. M. Bakr, Science **347**, 519 (2015).

[32] M. I. Saidaminov, A. L. Abdelhady, B. Murali, E. Alarousu, V. M. Burlakov, W. Peng, I. Dursun, L. Wang, Y. He, G. Maculan, A. Goriely, T. Wu, O. F. Mohammed, and O. M. Bakr, Nat. Commun. **6**, 7586 (2015).

[33] See Supplemental Material at http://link.aps.org/supplemental/10.1103/PhysRevMaterials.3.111601, which includes Refs. [34–38], for details of cleaved samples, x-ray Laue spectroscopy, *Z*-scan spectroscopy, excitation wavelength and fluence dependence of *Z*-scan measurement, analysis of *Z*-scan measurement, exciton reduced mass near the band edge and wave-number dependence of the wave function, and excitation-wavelength dependences of third-order nonlinear optical coefficients.

[34] B. S. Kalanoor, L. Gouda, R. Gottesman, S. Tirosh, E. Haltzi, A. Zaban, and Y. R. Tischler, ACS Photon. **3**, 361 (2016).

[35] P. Y. Yu and M. Cardona, *Fundamentals of Semiconductors: Physics and Materials Properties* (Springer, Berlin, 2001).

[36] R. S. Calsaverini, E. Bernardes, J. C. Egues, and D. Loss, Phys. Rev. B. **78**, 155313 (2008).

[37] A. L. Efros and M. Rosen, Annu. Rev. Mater. Sci. **30**, 475 (2000).

[38] J. Even, L. Pedesseau, J.-M. Jancu, and C. Katan, J. Phys. Chem. Lett. **4**, 2999 (2013).

[39] M. Sheik-Bahae, A. A. Said, T.-H. Wei, D. J. Hagan, and E. W. Van Stryland, IEEE J. Quantum Electron. **26**, 760 (1990).

[40] B. Gu, W. Ji, and X.-Q. Huang, Appl. Opt. **47**, 1187 (2008).

[41] E. W. Van Stryland, M. A. Woodall, H. Vanherzeele, and M. J. Soileau, Opt. Lett. **10**, 490 (1985).

[42] T. Umebayashi, K. Asai, T. Kondo, and A. Nakao, Phys. Rev. B **67**, 155405 (2003).

[43] J. Even, L. Pedesseau, C. Katan, M. Kepenekian, J-S. Lauret, D. Sapori, and E. Deleporte, J. Phys. Chem. C **119**, 10161 (2015).

[44] R. W. Boyd, *Nonlinear Optics*, 3rd ed. (Academic, New York, 2008).

[45] M. Sheik-Bahae, D. C. Hutchings, D. J. Hagan, and E. W. Van Stryland, IEEE J. Quantum Electron. **27**, 1296 (1991).

[46] H. Haug and S. W. Koch, *Quantum Theory of the Optical and Electronic Properties of Semiconductors* (World Scientific, Singapore, 1994).

[47] K. Galkowski, A. Mitioglu, A. Miyata, P. Plochocka, O. Portugall, G. E. Eperon, J. T.-W. Wang, T. Stergiopoulos, S. D. Stranks, H. J. Snaith, and R. J. Nicholas, Energy Environ. Sci. **9**, 962 (2016).

[48] Z. Yang, A. Surrente, K. Galkowski, A. Miyata, O. Portugall, R. J. Sutton, A. A. Haghighirad, H. J. Snaith, D. K. Maude, P. Plochocka, and R. J. Nicholas, ACS Energy Lett. **2**, 1621 (2017).

[49] K. Galkowski, A. Surrente, A. Miyata, M. Baranowski, B. Zhao, Z. Yang, A. Sadhanala, S. Mackowski, S. D. Stranks, and P. Plochocka, ACS Energy Lett. **4**, 615 (2019).